Hindawi
International Journal of Aerospace Engineering
Volume 2021, Article ID 2159674, 13 pages
https://doi.org/10.1155/2021/2159674

*Research Article*

# Real-Time Optimal Negotiation Mode Selection Based on Three-Way Decision for Decentralized Remote Sensing Satellite Cluster

**Xuelei Deng, Yunfeng Dong, and Chao Zhang**

*School of Astronautics, Beihang University, Beijing 100191, China*

Correspondence should be addressed to Yunfeng Dong; sinosat@buaa.edu.cn

Received 6 April 2021; Accepted 13 July 2021; Published 31 July 2021

Academic Editor: Hikmat Asadov



The mission planning for multisatellite is a complex optimization problem, which is sensitive to time delay caused by communication and decision. Different modes are suitable for different situations. Therefore, we design the workflows of three modes: the independence mode, the MAS mode, and the ground-based mode. And then, a real-time mode selection method based on the three-way decision is proposed to choose the best mode onboard. The experiments proved the effectiveness and advantage of our proposed method.

## 1. Introduction

Satellite remote sensing is aimed at obtaining information from the earth's surface and has been widely used in geography, earth science, meteorology, military, etc. [1]. Early remote sensing missions are accomplished by a single satellite, and the missions are usually planned offline. With the growing development of onboard hardware and software, some well-developed onboard mission planning systems are designed. For example, a remote agent technology-based mission planning system under an autonomous agent architecture was designed for DS-1 (Deep Space-1) [2, 3] to make itself intelligent [4]. The ASE [5, 6] (Autonomous Science craft Experiment) was another famous system used on EO-1 [7, 8] (Earth Observe). In August 2000, the ASPEN [9, 10] (Automated Planning/Scheduling Environment) was successfully used on CX-1 (Citizen Explorer).

The main disadvantage of single-satellite remote sensing is its long response time. One way to overcome it is to use a satellite cluster or satellite constellation. This, however, brings a new challenge to mission planning, i.e., to determine how different satellites cooperate to observe multiple targets. Researchers proposed many methods to address the above challenge. MAS (multiagent system) is the main solution to the distributed autonomy problem for multiple satellites. In order to get the balance between algorithm complexity and mission profit, the research on the MAS was carried out from two aspects. On the one hand, the researchers were devoted to applying the algorithms onboard. Heuristics algorithms are widely considered to be effective onboard [11]. Wang et al. [12] designed a cooperative coevolutionary algorithm and a novel fixed-length binary encoding mechanism for mission management, which can improve the efficiency of mission management. Morgan et al. [13] presented a decentralized, model predictive control algorithm to control hundreds to thousands of agents. Du and Li [14] proposed a new multidimensional and multiagent cluster collaboration model. The usage of contract net protocol-based secondary allocation strategy increased the observation benefit and reduced the impact of task conflicts. Cheng et al. [15] proposed and compared three negotiation models: acquaintance's trust-based announcing bidding, adaptive bidding with swarm intelligence, and a multiattribute decision-based fuzzy evaluation bidding method. The abovementioned methods prefer effectiveness to optimality and can be applied onboard. On the other hand, some researchers focused on mission profit including the coverage rate of targets and load balance. Iacopino et al. [16] designed an innovative self-organizing multiagent ground-based automated planning and scheduling architecture, inspired by ant colony optimization algorithms. Gallud and Selva [17] presented an agent-based simulation framework. The systems of observing

autonomous vehicles performing a set of observational tasks were verified on the framework. Globus et al. [18] applied and compared the genetic algorithm, simulated annealing, squeaky wheel optimization, and stochastic hill-climbing methods, which solve the scheduling problem effectively, and simulated annealing with 1-9 random swaps performed the best. However, these methods can hardly be used onboard considering computation and communication limitations. In addition, these methods may become unstable in the case of time delay.

The above researches mainly focused on either the efficiency or the optimality of the MAS. However, as far as we know, there is few research aimed at balancing the two sides. In fact, efficiency and optimality can be achieved under certain situations. When communication is unavailable or the sensing mission is urgent, the satellite only concerns itself, which is similar to the single-satellite mission planning situation. On the contrary, when communication is available or consistency is achievable, multiple satellites should work as a cluster and the mission should be planned corporately.

In this paper, we propose a multimode method based on the three-way decision under a decentralized architecture. Firstly, we establish a multimode negotiation model which consists of three modes: the independence mode, MAS mode (multiagent system mode), and the ground-based mode. In the independence mode, the satellite finishes the mission planning and the observation all by itself. In the MAS mode, the satellite works as an agent and negotiates with each other to manage the missions. In the ground-based mode, the information of satellites and missions are both sent to the ground station similar to [19, 20]. Three modes are switched according to communication delay. Then, algorithms outstanding on the coverage rate of targets and load balance are used. Secondly, we use the three-way decision method to intelligently select the best mode from the three modes. More specifically, we simulate the ground-based mode and the MAS mode with different time delays as samples. Then, we cluster the mission selections in these samples to find out the boundaries between each mode. The envelopes of boundaries with different time delays are found out. They divide the mission selections into several areas, including the certain areas and the fuzzy areas. The certain area belongs to one mode for sure. And the fuzzy area belongs to more than one mode. Different strategies are used in different areas.

The remainder of the paper is organized as follows. In Section 2, the problem of mission management is introduced. In Section 3, the workflow of each mode is designed. In Section 4, an intelligently real-time mode selection method based on the three-way decision is proposed. In Section 5, experiments are carried out to verify this method in different conditions. Finally, the conclusions of the study are given in Section 6.

## 2. The Proposed Approach

Suppose there are $M$ satellites and $N$ targets. The $x_{k,i,j}$ is one selection of the $j$th mission of the $i$th target for $k$th satellite, where $k \in [1, M]$, $i \in [1, N]$, $j \in [1, 5]$. $j$ is the index of mission stages which are discovery, identification, confirmation, tracking, and monitoring. $x_{k,i,j} = 1$ when the $k$th satellite selects the $j$th mission of the $i$th target. Therefore, the mission management problem of satellite cluster can be described as

$$\begin{aligned} \text{find}: &\quad X, \\ \max: &\quad \sum_{k=1}^{M}\sum_{i=1}^{N}\sum_{j=1}^{5} P_{i,j}x_{k,i,j}, x_{k,i,j} \in X, \\ s.t.: &\quad C_{o_i}(t) = 1, \\ &\quad C_{g_i}(t) = 1, \\ &\quad C_{T_i}(t) = 1, \end{aligned} \tag{1}$$

where $X$ is the mission selection matrix, and $x_{k,i,j}$ is one element in the $X$. $P_{i,j}$ is the mission profit defined in [21]. The optical visibility constraint $C_{o_i}(t)$ and the geometric visibility constraint $C_{g_i}(t)$ are calculated the same as [21]. The time constraint $C_{T_i}(t)$ is described as

$$C_{T_i}(t) = \begin{cases} 1, & \text{To}_i + Td_i + Tp_i < Tw_i, \\ 0, & \text{else}, \end{cases} \tag{2}$$

where $\text{To}_i$ is the mission origin time of the $i$th mission. $Td_i$ is the time delay of the negotiation process. $Tp_i$ is the preparation time of $i$th mission, including the satellite switch mode time, attitude maneuver time, and payload prepare time. $Tw_i$ is the start time of observe window of the $i$th mission.

To manage missions on different situations, a multimode method is developed. Firstly, three effective modes are established: an independent mode, a ground-based mode, and a MAS mode. Dynamic programming is used in the ground-based mode to search for the optimal solution. A two-level negotiation method is used in the MAS mode. After that, motion planning for a single satellite is used to adjust the mission sequence dynamically. Secondly, we use the three-way decision method to distinguish the best mode for different missions. We sample the mission selection by different time delays. Mission clustering is used to find the boundaries between modes. Then, the envelopes are found out and divide the missions into several certain areas and fuzzy areas. Different strategies are applied to different areas. The flowchart of the multimode architecture proposed in this paper is illustrated in Figure 1.

## 3. Multimode Negotiation Model

We propose a space-ground integrated decentralized framework, shown in Figure 2. The satellite cluster can be divided into several domains. In each domain, the satellites form a small decentralized network. Two consistency algorithms [22] and PBFT [23] of the private chain are suitable for a single domain. Satellites play different roles: leader node (*Leader*) or follower node (*Follower*). The *Leader* is responsible for managing its *Follower*s in the domain and communicates with other *Leader*s in other domains and the ground stations. Each *Follower* can originate missions and request for negotiation. The *Leader*s form a large decentralized

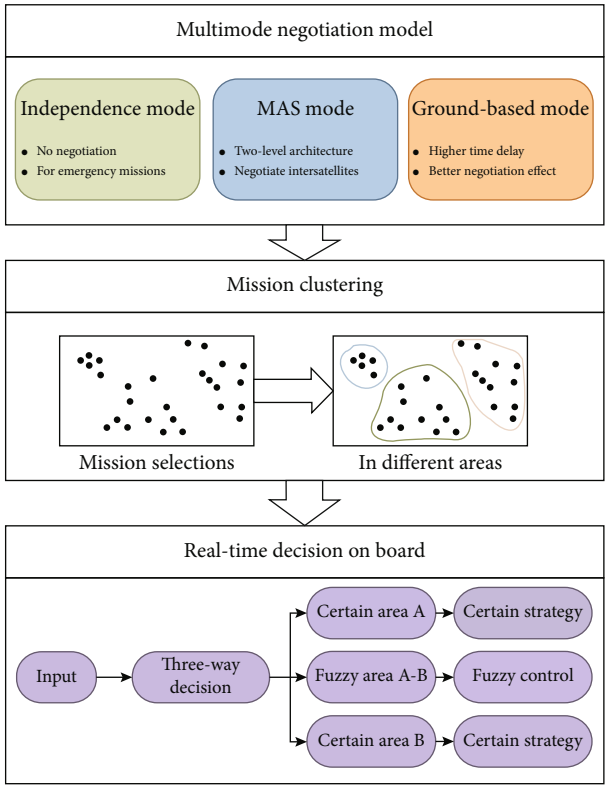


Figure 1: The flowchart of the multimode method.

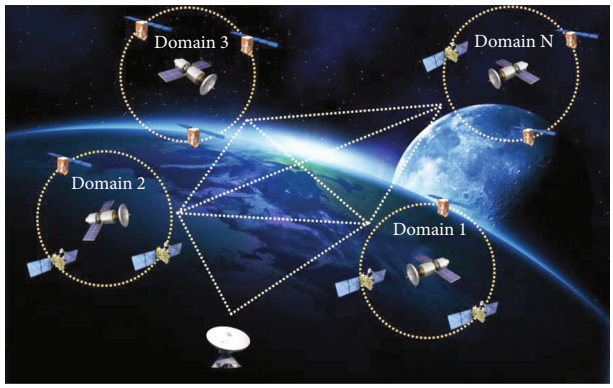


Figure 2: The architecture of decentralized satellite clusters.

network that connects all domains. Two consistency algorithms (DPOS [24] and RIPPLE [24]) of the alliance chain are suitable for interdomain decentralization. The architecture of negotiation has two levels. In the first level, the satellites reach an agreement in each domain. In the second level, satellites reach an agreement among the domains. The ground station is a cloud server in the system, which can support some complex ground-based algorithms.

We evaluate missions with two properties: urgency and significance. Then, the best mode to manage the mission is selected on board. For emergency missions, the best choice is the independent mode without negotiation. For the ground-based mode, the mission information and the satellite status are both sent to the ground station. The satellites follow the command of the ground station. For the MAS mode, the decision is made by all *Leaders* of domains. The satellites follow the command of their *Leader*.

*3.1. Ground-Based Mode.* The ground-based mode uses the cloud server of the ground station to complete the mission management requested by the satellites, which is suitable for the important and less urgent missions. There are many factors considered in ground cloud planning, including constraints such as payload working duration, memory, power, and thermal status. Dynamic programming algorithm is applied in solution. The process is shown in Figure 3.

(i) Step1: mission origin. The mission origin behaviour of each satellite is automatically triggered when there is no mission. The behaviour is a one-time behaviour and is removed after completion. Firstly, the satellites perform the orbit recursion and coordinate system transformation. Secondly, the observation time windows are calculated according to the relative position between the satellite and the targets. Finally, the profit and cost of each time window are calculated

(ii) Step2: mission submission. The status of the satellite and the missions suitable for ground-based mode is submitted to the *Leader*, which includes the remaining working duration of the payload, the remaining capacity, the remaining power, target ID, mission type, expected time window, and other parameters

(iii) Step3: mission delivery. The *Leader* delivers the mission status to the ground station

(iv) Step4: mission assignment. The ground station starts the mission assignment when there are no new requests delivered for some time or the first request has been idle for some time. The assignment is regarded as a knapsack problem, and the dynamic programming algorithm is applied. The infeasible solutions are removed

(v) Step5: release result. The mission assignment results are released to the *Leaders*, and the *Leader* releases the results to the *Followers*

(vi) Step6: result check and execute. The satellites receive the assignment results and verify the feasibility of the results. The satellites execute missions if feasible. If not, the satellites pick as many missions as they can and feed the failure reason back to the ground for correction. The selection of the $k$th satellite onboard can be described as

$$\begin{aligned} \text{find}: &\quad X_k, \\ \max: &\quad \sum_{i=1}^{N}\sum_{j=1}^{5} P_{i,j}x_{i,j}, x_{i,j} \in X_k \\ s.t.: &\quad \sum_{i=1}^{N}\sum_{j=1}^{5} c_{i,j}x_{i,j} < c_{\max}, \end{aligned} \tag{3}$$

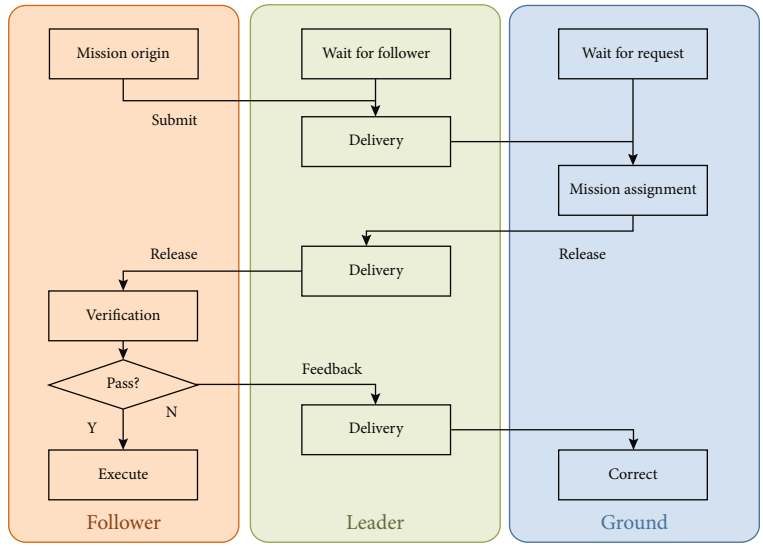


Figure 3: Ground-based mode process.

where $c_{i,j}$ is the mission cost of the $j$th mission of the $i$th target for the $k$th satellite, $c_{\max}$ is the max cost that the $k$th satellite can afford.

*3.2. Multiagent System Mode.* In the MAS mode, all satellites are regarded as agents, which can origin missions and request for negotiation. A two-level negotiation architecture is designed. The satellites of each domain calculate all possible time windows and negotiate with each other. After consistency is reached in domain, the Leaders start to negotiate with each other. The process can be divided into the following steps shown in Figure 4:

(i) Step1: mission origin. Same as before

(ii) Step2: mission submission. The missions suitable for the MAS mode are sent to the cluster leader, including the start time and duration of the time window, mission type, mission profit, and mission cost

(iii) Step3: mission assignment in the domain. The *Leader* is responsible for processing the received task requests periodically. A dynamic programming algorithm is used in this step. The best solution is found and recorded in the block

(iv) Step4: result block verification. In order to avoid errors in mission assignment, the temporary block should be published in the domain first and be verified by *Follower*s in the domain before the next step. The verification basis is as follows:

(1) *Follower* only verifies missions related to itself

(2) *Follower* compares the submitted mission set with the result block. When the mission set in the result block is a subset of the submitted mission set and is not empty, the verification is passed

(3) The sum of the execution cost of all missions in the result block is no more than the max cost that satellite can afford

If the verification is passed, the missions are released to the domains, then go to Step6 for inter-domain negotiation. If not, go to Step5.

(v) Step5: mission adjusting. The missions should be adjusted according to the problems. The possible problems and corresponding treatment strategies are as follows:

(1) The mission set in the result block contains missions not belong to the submitted mission set, the mission should be deleted

(2) The mission set for some *Follower*s in the result block is empty. The mission assignment process runs again only for all the *Follower*s with an empty mission set

(3) The total cost of the mission exceeds the capabilities of the satellite

The missions of the satellite sort missions according to the cost-effectiveness ratio, and the missions with a high cost-effectiveness ratio are given up. Go back to Step4.

(vi) Step6: negotiation between clusters. The DPOS decentralized algorithm is used among domains, which means that the *Leader*s of each domain form a leader group, and one *Leader* is voted to be the president of that group. All *Leader*s in the group participate in the negotiation and generate the result block at the same time

(vii) Step7: verification interdomain. The president of the leader group has the authority to release the

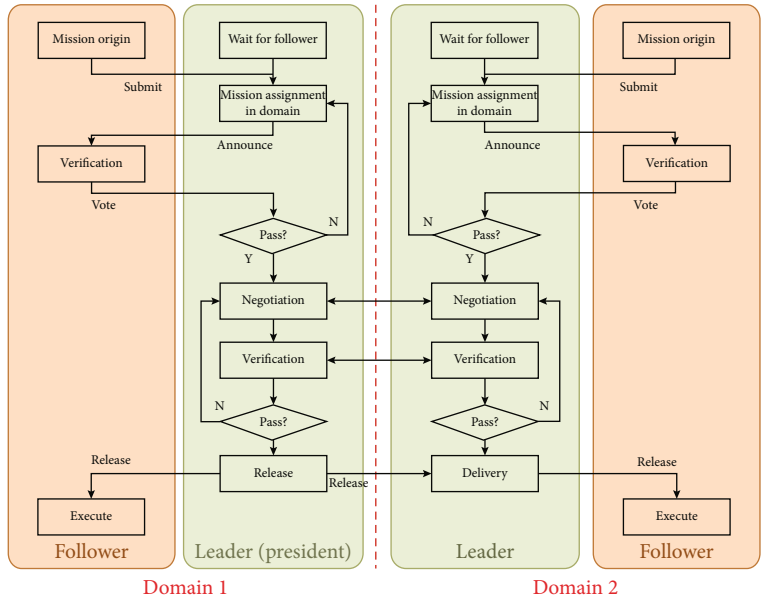


Figure 4: MAS mode process.

result block. It transfers the block in the leader group first. All *Leaders* in the group compare the local result block and the received result block. Then, the compare result is recorded as positive if the same or negative if not

(viii) Step8: Result release. If more than half of *Leaders* vote positive, the result block is considered correct. The president of the leader group releases the block in the leader group. The *Leaders* release the result block in their own domain

## 4. Real-Time Mode Selection

The satellite needs to select an appropriate mode for each mission. Mode selection is also difficult because the time delay is mainly caused by communication and the decision is random, which is related to the number of total missions. Thus, we cluster the missions in three modes to find certain areas and fuzzy areas. Then, we use the three-way decision method to simplify the decision in a certain area, which can use linear formula. The satellites focus on the decision in the fuzzy area using fuzzy control.

*4.1. Sample Collection.* The time delay constraint can be described as

$$\begin{cases} \mathrm{To}_i + Tg_i + Tp_i < Tw_i, \\ \mathrm{To}_i + Tm_i + Tp_i < Tw_i, \end{cases} \tag{4}$$

where $Tg_i$ is the time delay of the ground-based mode, and $Tm_i$ is the time delay of the MAS mode.

There are two influence factors of the time delay of the ground-based mode and the MAS mode. The first one is the number of the decision missions, which affects the bandwidth during communication and processing time during decision. The second one is the environment factor, which is random. Thus, the actual time delay can be described as

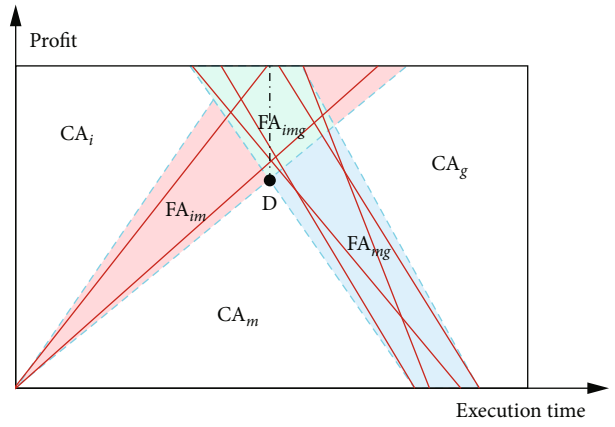


Figure 5: The areas of the mission property space.

$$\begin{cases} Tg_i = T_g^{(n)} + T_g^{(r)}, \\ Tm_i = T_m^{(n)} + T_m^{(r)}, \end{cases} \tag{5}$$

where $T_g^{(n)}$ is the time delay of the normal decision in the ground-based mode. $T_g^{(r)}$ is the random time delay of the ground-based mode. $T_m^{(n)}$ is the time delay of the normal decision in the MAS mode. $T_m^{(r)}$ is the random time delay of the MAS mode.

We firstly test the processing time of mission assignment algorithms in both modes. The values of $T_g^{(n)}$ and $T_m^{(n)}$ depend on the test result. The values of $T_g^{(r)}$ and $T_m^{(r)}$ are set

Table 1: Temperature and wildlife count in the three areas covered by the study.

| Target ID | Position | Course angle (°) | Velocity (knot) | Mission initial profit |
|---|---|---|---|---|
| 1 | 128.08°E, 25.61°N | -135 | 3.2 | 10 |
| 2 | 131.32°E, 11.33°S | -23 | 16.3 | 7 |
| 3 | 143.65°E, 16.19°N | 56 | 8.6 | 5 |
| … | … | … | … | … |

Table 2: Parameters for satellite 1.

| Category | Parameter | Value |
|---|---|---|
| Orbit parameter | Semimajor axis (m) | 6878000 |
| | Eccentricity | 0 |
| | Inclination (°) | 56 |
| | RAAN (°) | 80 |
| | Argument of perigee (°) | 0 |
| | True anomaly (°) | 130 |
| Attitude parameter | Agile | Y |
| | Max. maneuver angle | 45 |
| | Angular velocity | 1 |
| | Angular acceleration | 0.1 |
| | Maneuver mode | Trapezoid method |
| Payload parameter | Imaging width (km) | 4 |
| | Image size per frame (Mb) | 6.4 |

by experience. Thus, the ranges of $Tg$ and $Tm$ are determined. The section method is used to divide the time delay into several parts. Thus, we get the total profit of each mode with different time delays as samples.

*4.2. Mission Clustering.* Mission clustering is aimed at finding the best boundary of each mode. We describe the boundary as a linear function. For the independence mode and the MAS mode, we should find a boundary in order to maximize the profit summary. The profit summary consists of two parts. One is the missions on the left of the boundary in the independence mode. The other is the missions on the right of the boundary in the MAS mode. This process can be described as

$$\begin{aligned} \text{find}: &\quad k_l, b_l, \\ \max: &\quad \sum_{i=1}^{N^{(\text{in})}} P_i^{(\text{in})} + \sum_{j=1}^{N^{(m)}} P_j^{(m)}, \\ s.t.: &\quad P_i^{(\text{in})} > k_l t_i^{(\text{in})} + b_l, \\ &\quad P_j^{(m)} < k_l t_j^{(m)} + b_l, \\ &\quad k_l > 0, \end{aligned} \tag{6}$$

where $N^{(\text{in})}$ is the number of missions in the independence mode. $P_i^{(\text{in})}$ is the $i$th mission's profit in the independence mode. $t_i^{(\text{in})}$ is the execution time of the $i$th mission in the independence mode. $N^{(m)}$ is the number of missions in the MAS mode, and $P_j^{(m)}$ is the $j$th mission's profit in the MAS mode. $t_j^{(m)}$ is the execution time of the $j$th mission in the MAS mode.

The missions in the sample are discrete; therefore, there might be several solutions in one condition. Besides the multiple samples, we can get a set of boundaries, shown as the red line on the left in Figure 5. We pick the envelope as the boundary of the certain area, shown as the blue dotted line on the left in Figure 5.

We also obtain the boundary of the MAS mode and the ground-based mode, which can be described as

$$\begin{aligned} \text{find}: &\quad k_r, b_r, \\ \max: &\quad \sum_{i=1}^{N^{(g)}} P_i^{(g)} + \sum_{j=1}^{N^{(m)}} P_j^{(m)}, \\ s.t.: &\quad P_i^{(g)} > k_r t_i^{(g)} + b_r, \\ &\quad P_j^{(m)} < k_r t_j^{(m)} + b_r, \\ &\quad k_r < 0, \end{aligned} \tag{7}$$

where $N^{(g)}$ is the number of missions in the ground-based mode. $P_i^{(g)}$ is the $i$th mission's profit in the ground-based mode. $t_i^{(g)}$ is the execution time of the $i$th mission in the ground-based mode. we can get a set of boundaries, shown

Table 3: The orbit parameters of all satellites.

| Satellite ID | Semimajor axis (m) | Eccentricity | Inclination (°) | RAAN (°) | Argument of perigee (°) | True anomaly (°) |
|---|---|---|---|---|---|---|
| 1 | 6878000 | 0 | 40 | 80 | 0 | 130 |
| 2 | 6878000 | 0 | 40 | 80 | 0 | 125 |
| 3 | 6878000 | 0 | 40 | 80 | 0 | 120 |
| 4 | 6878000 | 0 | 40 | 80 | 0 | 115 |
| 5 | 6878000 | 0 | 40 | 80 | 0 | 110 |
| 6 | 6878000 | 0 | 40 | 80 | 0 | 70 |
| 7 | 6878000 | 0 | 40 | 80 | 0 | 65 |
| 8 | 6878000 | 0 | 40 | 80 | 0 | 60 |
| 9 | 6878000 | 0 | 40 | 80 | 0 | 55 |
| 10 | 6878000 | 0 | 40 | 80 | 0 | 50 |
| 11 | 6878000 | 0 | 40 | 80 | 0 | 10 |
| 12 | 6878000 | 0 | 40 | 80 | 0 | 5 |
| 13 | 6878000 | 0 | 40 | 80 | 0 | 0 |
| 14 | 6878000 | 0 | 40 | 80 | 0 | -5 |
| 15 | 6878000 | 0 | 40 | 80 | 0 | -10 |
| 16 | 6878000 | 0 | 40 | 80 | 0 | -50 |
| 17 | 6878000 | 0 | 40 | 80 | 0 | -55 |
| 18 | 6878000 | 0 | 40 | 80 | 0 | -60 |
| 19 | 6878000 | 0 | 40 | 80 | 0 | -65 |
| 20 | 6878000 | 0 | 40 | 80 | 0 | -70 |
| 21 | 6878000 | 0 | 40 | 80 | 0 | -110 |
| 22 | 6878000 | 0 | 40 | 80 | 0 | -115 |
| 23 | 6878000 | 0 | 40 | 80 | 0 | -120 |
| 24 | 6878000 | 0 | 40 | 80 | 0 | -125 |
| 25 | 6878000 | 0 | 40 | 80 | 0 | -130 |
| 26 | 6878000 | 0 | 40 | 80 | 0 | -170 |
| 27 | 6878000 | 0 | 40 | 80 | 0 | -175 |
| 28 | 6878000 | 0 | 40 | 80 | 0 | -180 |
| 29 | 6878000 | 0 | 40 | 80 | 0 | -185 |
| 30 | 6878000 | 0 | 40 | 80 | 0 | -190 |
| 31 | 6878000 | 0 | 40 | 170 | 0 | 145 |
| 32 | 6878000 | 0 | 40 | 170 | 0 | 140 |
| 33 | 6878000 | 0 | 40 | 170 | 0 | 135 |
| 34 | 6878000 | 0 | 40 | 170 | 0 | 130 |
| 35 | 6878000 | 0 | 40 | 170 | 0 | 125 |
| 36 | 6878000 | 0 | 40 | 170 | 0 | 85 |
| 37 | 6878000 | 0 | 40 | 170 | 0 | 80 |
| 38 | 6878000 | 0 | 40 | 170 | 0 | 75 |
| 39 | 6878000 | 0 | 40 | 170 | 0 | 70 |
| 40 | 6878000 | 0 | 40 | 170 | 0 | 65 |
| 41 | 6878000 | 0 | 40 | 170 | 0 | 25 |
| 42 | 6878000 | 0 | 40 | 170 | 0 | 20 |
| 43 | 6878000 | 0 | 40 | 170 | 0 | 15 |
| 44 | 6878000 | 0 | 40 | 170 | 0 | 10 |
| 45 | 6878000 | 0 | 40 | 170 | 0 | 5 |
| 46 | 6878000 | 0 | 40 | 170 | 0 | -35 |
| 47 | 6878000 | 0 | 40 | 170 | 0 | -40 |
| 48 | 6878000 | 0 | 40 | 170 | 0 | -45 |

Table 3: Continued.

| Satellite ID | Semimajor axis (m) | Eccentricity | Inclination (°) | RAAN (°) | Argument of perigee (°) | True anomaly (°) |
|---|---|---|---|---|---|---|
| 49 | 6878000 | 0 | 40 | 170 | 0 | -50 |
| 50 | 6878000 | 0 | 40 | 170 | 0 | -55 |
| 51 | 6878000 | 0 | 40 | 170 | 0 | -95 |
| 52 | 6878000 | 0 | 40 | 170 | 0 | -100 |
| 53 | 6878000 | 0 | 40 | 170 | 0 | -105 |
| 54 | 6878000 | 0 | 40 | 170 | 0 | -110 |
| 55 | 6878000 | 0 | 40 | 170 | 0 | -115 |
| 56 | 6878000 | 0 | 40 | 170 | 0 | -155 |
| 57 | 6878000 | 0 | 40 | 170 | 0 | -160 |
| 58 | 6878000 | 0 | 40 | 170 | 0 | -165 |
| 59 | 6878000 | 0 | 40 | 170 | 0 | -170 |
| 60 | 6878000 | 0 | 40 | 170 | 0 | -175 |
| 61 | 6878000 | 0 | 40 | 260 | 0 | 160 |
| 62 | 6878000 | 0 | 40 | 260 | 0 | 155 |
| 63 | 6878000 | 0 | 40 | 260 | 0 | 150 |
| 64 | 6878000 | 0 | 40 | 260 | 0 | 145 |
| 65 | 6878000 | 0 | 40 | 260 | 0 | 140 |
| 66 | 6878000 | 0 | 40 | 260 | 0 | 100 |
| 67 | 6878000 | 0 | 40 | 260 | 0 | 95 |
| 68 | 6878000 | 0 | 40 | 260 | 0 | 90 |
| 69 | 6878000 | 0 | 40 | 260 | 0 | 85 |
| 70 | 6878000 | 0 | 40 | 260 | 0 | 80 |
| 71 | 6878000 | 0 | 40 | 260 | 0 | 40 |
| 72 | 6878000 | 0 | 40 | 260 | 0 | 35 |
| 73 | 6878000 | 0 | 40 | 260 | 0 | 30 |
| 74 | 6878000 | 0 | 40 | 260 | 0 | 25 |
| 75 | 6878000 | 0 | 40 | 260 | 0 | 20 |
| 76 | 6878000 | 0 | 40 | 260 | 0 | -20 |
| 77 | 6878000 | 0 | 40 | 260 | 0 | -25 |
| 78 | 6878000 | 0 | 40 | 260 | 0 | -30 |
| 79 | 6878000 | 0 | 40 | 260 | 0 | -35 |
| 80 | 6878000 | 0 | 40 | 260 | 0 | -40 |
| 81 | 6878000 | 0 | 40 | 260 | 0 | -80 |
| 82 | 6878000 | 0 | 40 | 260 | 0 | -85 |
| 83 | 6878000 | 0 | 40 | 260 | 0 | -90 |
| 84 | 6878000 | 0 | 40 | 260 | 0 | -95 |
| 85 | 6878000 | 0 | 40 | 260 | 0 | -100 |
| 86 | 6878000 | 0 | 40 | 260 | 0 | -140 |
| 87 | 6878000 | 0 | 40 | 260 | 0 | -145 |
| 88 | 6878000 | 0 | 40 | 260 | 0 | -150 |
| 89 | 6878000 | 0 | 40 | 260 | 0 | -155 |
| 90 | 6878000 | 0 | 40 | 260 | 0 | -160 |
| 91 | 6878000 | 0 | 40 | 350 | 0 | 175 |
| 92 | 6878000 | 0 | 40 | 350 | 0 | 170 |
| 93 | 6878000 | 0 | 40 | 350 | 0 | 165 |
| 94 | 6878000 | 0 | 40 | 350 | 0 | 160 |
| 95 | 6878000 | 0 | 40 | 350 | 0 | 155 |
| 96 | 6878000 | 0 | 40 | 350 | 0 | 115 |

Table 3: Continued.

| Satellite ID | Semimajor axis (m) | Eccentricity | Inclination (°) | RAAN (°) | Argument of perigee (°) | True anomaly (°) |
|---|---|---|---|---|---|---|
| 97 | 6878000 | 0 | 40 | 350 | 0 | 110 |
| 98 | 6878000 | 0 | 40 | 350 | 0 | 105 |
| 99 | 6878000 | 0 | 40 | 350 | 0 | 100 |
| 100 | 6878000 | 0 | 40 | 350 | 0 | 95 |
| 101 | 6878000 | 0 | 40 | 350 | 0 | 55 |
| 102 | 6878000 | 0 | 40 | 350 | 0 | 50 |
| 103 | 6878000 | 0 | 40 | 350 | 0 | 45 |
| 104 | 6878000 | 0 | 40 | 350 | 0 | 40 |
| 105 | 6878000 | 0 | 40 | 350 | 0 | 35 |
| 106 | 6878000 | 0 | 40 | 350 | 0 | -5 |
| 107 | 6878000 | 0 | 40 | 350 | 0 | -10 |
| 108 | 6878000 | 0 | 40 | 350 | 0 | -15 |
| 109 | 6878000 | 0 | 40 | 350 | 0 | -20 |
| 110 | 6878000 | 0 | 40 | 350 | 0 | -25 |
| 111 | 6878000 | 0 | 40 | 350 | 0 | -65 |
| 112 | 6878000 | 0 | 40 | 350 | 0 | -70 |
| 113 | 6878000 | 0 | 40 | 350 | 0 | -75 |
| 114 | 6878000 | 0 | 40 | 350 | 0 | -80 |
| 115 | 6878000 | 0 | 40 | 350 | 0 | -85 |
| 116 | 6878000 | 0 | 40 | 350 | 0 | -125 |
| 117 | 6878000 | 0 | 40 | 350 | 0 | -130 |
| 118 | 6878000 | 0 | 40 | 350 | 0 | -135 |
| 119 | 6878000 | 0 | 40 | 350 | 0 | -140 |
| 120 | 6878000 | 0 | 40 | 350 | 0 | -145 |

as the red line on the left in Figure 5. We pick the envelope as the boundary of the certain area, shown as the blue dotted line on the left in Figure 5.

*4.3. Three-Way Decision for Mode Selection.* The three-way decision is proposed by Yao [25–27]. The basic idea is to divide a complex problem to three domains, which can be described as two certain problems and one fuzzy problem. Different strategies are used in different problems, which reduce the cost and time of decision.

We preserve the envelopes, which divide the space into six areas. These six areas are either *certain areas* or *fuzzy areas*. The left area $\mathbf{CA}_i$ is the *certain area* of the independence mode. $\mathbf{CA}_m$ in the middle is the *certain area* of the MAS mode. The right area $\mathbf{CA}_g$ is the *certain area* of the ground-based mode. The red area $\mathbf{FA}_{im}$ is the *fuzzy area* to select from the independence mode or the MAS mode. The blue area $\mathbf{FA}_{mg}$ is the *fuzzy area* to select from the MAS mode or the ground-based mode. The green area $\mathbf{FA}_{img}$ is the *fuzzy area* to select from all three modes.

For the *fuzzy area* $\mathbf{FA}_{im}$, we use the fuzzy control method. The membership can be described as

$$\mathrm{A}_i^{(im)} = \frac{d_i^{(l)}}{d_i^{(l)} + d_i^{(r)}}, \tag{8}$$

Table 4: Random time delay of the MAS mode for simulation.

| Group ID | 1 | 2 | 3 | 4 | 5 | 6 |
|---|---|---|---|---|---|---|
| Random time delay (min) | 0 | 0.4 | 0.8 | 1.2 | 1.6 | 2 |

Table 5: Random time delay of the ground-based mode for simulation.

| Group ID | 1 | 2 | 3 | 4 | 5 | 6 | 7 | 8 |
|---|---|---|---|---|---|---|---|---|
| Random time delay (min) | 0 | 0.5 | 1 | 1.5 | 2 | 3 | 4 | 5 |

where $A_i^{(im)}$ is the membership of the $i$th mission in the *fuzzy area* $\mathbf{FA}_{im}$, $d_i^{(l)}$ is the distance from the $i$th mission point in space to the left envelope, and $d_i^{(r)}$ is the distance from the $i$th

$$\mathrm{mode}_i = \begin{cases} \text{independence mode}, & \mathrm{A}_i^{(im)} < \dfrac{2N_m}{N}, \\ \text{MAS mode}, & \text{else}, \end{cases} \tag{9}$$

where $\mathrm{mode}_i$ is the $i$th mission's mode. $N_m$ is the number of missions in the MAS mode, which varies during selection. $N$ is the total mission number.

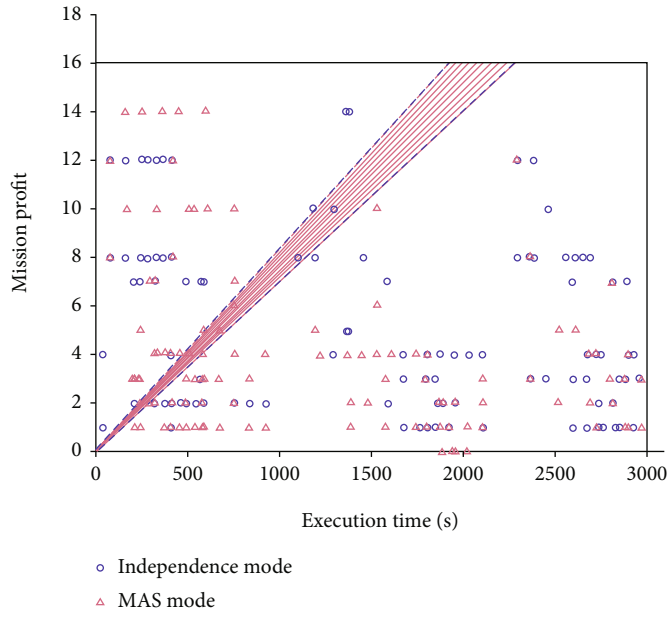


Figure 6: The boundaries and envelopes of the clustering result of the independence mode and the MAS mode.

For the *fuzzy area* $\mathbf{FA}_{mg}$, we also use the fuzzy control method. The membership's definition $A_i^{(mg)}$ is same as $A_i^{(im)}$. The mode selection can be described as

$$\text{mode}_i = \begin{cases} \text{MAS mode}, & \text{A}_i^{(mg)} < \dfrac{2N_g}{N} \\ \text{ground\_based mode}, & \text{else}, \end{cases} \tag{10}$$

where $N_g$ is the number of missions in the ground-based mode, which varies during selection.

For the *fuzzy area* $\mathbf{FA}_{img}$, we first find out the crossover point $D$, which is also the crossover point of the right envelope of the $\mathbf{FA}_{im}$ and the left envelope of the $\mathbf{FA}_{mg}$. Suppose $T_D$ as the execution time of the crossover point $D$ shown in Figure 5. Therefore, the *fuzzy area* $\mathbf{FA}_{img}$ can be divided into two parts by the function $t_i = T_D$ (the dotted line shown in Figure 5). The strategy of the *fuzzy area* $\mathbf{FA}_{img}$ can be described as

$$\text{mode}_i = \begin{cases} \text{MAS mode}, & t_i \le T_D \text{ and } N_m < \dfrac{N}{3}, \\ \text{ground\_based mode}, & t_i > T_D \text{ and } N_g < \dfrac{N}{3}, \\ \text{independence mode}, & \text{else}, \end{cases} \tag{11}$$

### 4.4. Experiments and Analyses

*4.4.1. Experimental Data.* We randomly generated a set of 77 ship targets. The target's motion is also random including course angle $\psi_i$ between -180° and 180° and velocity $v_i$ between 0 and 30 knots. Part of the targets is shown in Table 1.

Satellite parameters are shown in Table 2. There are 120 isomorphic satellites in the scene, consisting of 24 domains with 5 satellites in each of them. The middle nodes of the domains form a 24-node walker constellation in 6 orbit planes. The interval phase between two adjacent satellites in one domain is 5°. The detailed orbit parameters of all satellites are shown in Table 3.

*4.4.2. Sample Collection.* We set different time delays for the MAS mode shown in Table 4. And the ground-based mode and target number is shown in Table 5.

We collect 6 samples for the MAS mode and 8 samples for the ground-based mode. We collect 1 sample for the independence mode because there is no negotiation.

*4.4.3. Mission Clustering.* Firstly, we cluster the mission selections in each sample of the independence mode and the MAS mode. Therefore, we get $1 \times 6 = 6$ groups of boundaries and their envelopes, shown in Figure 6. The blue circles denote the missions in the sample of the independence mode. The red triangles denote the missions in the 6 samples of the MAS mode.

Secondly, we cluster the mission selections in each sample of the MAS mode and the ground-based mode in the same way. Therefore, we get $6 \times 8 = 48$ groups of boundaries and their envelopes, shown in Figure 7. The red triangles denote the missions in the 6 samples of MAS mode. The black pentagrams denote the missions in the sample of ground-based mode.

Finally, we obtain the three certain areas and three fuzzy areas shown in Figure 8.

## 5. Experiment Result

We apply all three modes and the multimode, with a 1-minute time delay of the MAS mode and a 2.5-minute time

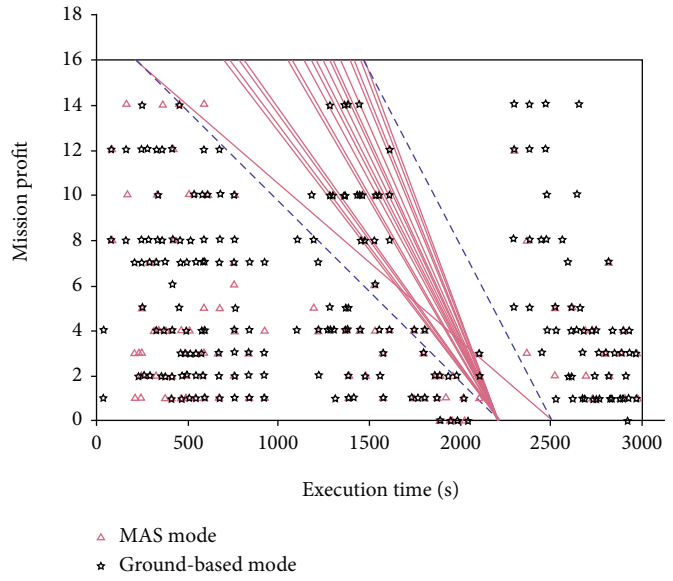


Figure 7: The boundaries and envelopes of the clustering result of the MAS mode and the ground-based mode.

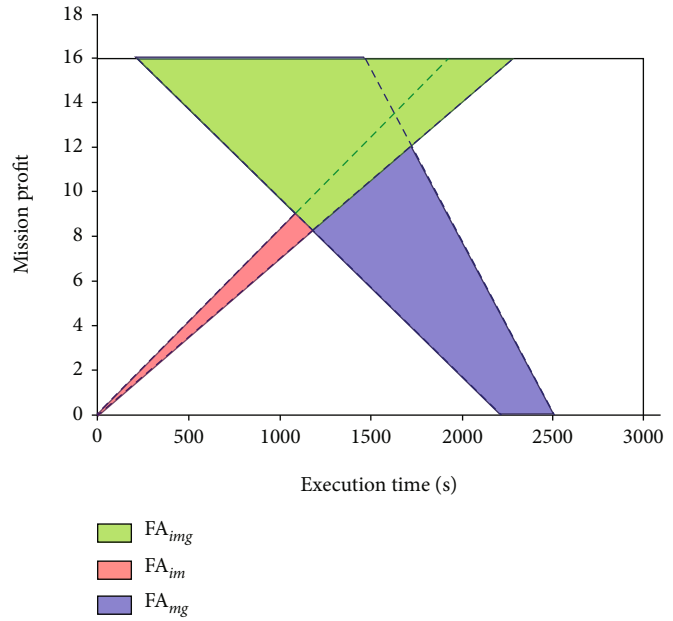


Figure 8: Three certain areas and three fuzzy areas.

delay of the ground-based mode. The profits of the missions are shown in Figure 9.

Comparison of the profits of all modes is presented in Figure 9. It can be seen that the multimode method can get the highest profit throughout the observation. The profits of the ground-based mode and the MAS mode do not increase at the beginning because of the delay of communication and decision. Therefore, the simulation result matches well with the expected result, which validates the multimode method.

In order to get higher profit with limited resources of communication and computation, a multimode method is proposed. We compare the multi-mode method with the traditional methods of the three modes, including the independence mode, the MAS mode, and the ground-based mode. The profits of the missions are shown in Figure 9. Three conclusions can be obtained:

(1) The multimode method performs best among these modes

(2) Because of the time delay, some missions failed at the beginning in the MAS system mode and the ground-based mode

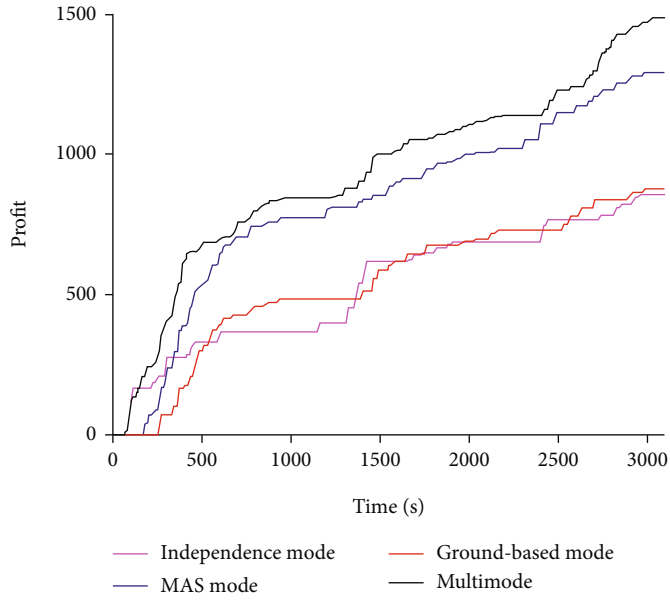


Figure 9: The profits of all modes.

(3) The ground-based mode performs worse than the MAS mode, which is mainly because of the higher time delay

To make real-time decisions of mode selection onboard, we divide the mission selections clustering into two parts. One is for the independence mode and the MAS mode; the other is for the MAS mode and the ground-based mode. Then, we get two sets of boundaries. The mission properties space can be divided into six areas, including three *certain area*s and three *fuzzy area*s, which is the same as expected.

## 6. Conclusions

Because of the limited computation ability and communication ability, some multiagent system algorithms are hardly used onboard. Therefore, keeping the balance of the profit and algorithm complexity attracts our attentions. In this paper, a multimode method based on the three-way decision under decentralized architecture is proposed, which is proved to be effective. The advantages of the proposed method are summarized as follows:

(1) The three modes perform differently with different time delays. We propose a multimode method to use different modes for different missions, which brings better profit

(2) The selection of mode may take some time, which also causes time delay. Therefore, the three-way decision method is used to simplify the decision-making process and make a real-time selection

(3) A decentralized network consisting of 120 satellites is established in the scene, which might be extensible to larger satellite clusters in the future

## Data Availability

The data used to support the findings of this study are available from the corresponding author upon request.

## Conflicts of Interest

The authors declare that they have no conflicts of interest.

## Acknowledgments

This research was funded by the National Key Research and Development Program of China (No. 2016YFB0501102).

## References

[1] G. R. van der Werf, J. T. Randerson, L. Giglio et al., "Global fire emissions and the contribution of deforestation, savanna, forest, agricultural, and peat fires (1997–2009)," *Atmospheric Chemistry and Physics*, vol. 10, no. 23, pp. 11707–11735, 2010.

[2] G. Rabideau, R. Knight, S. Chien, A. Fukunaga, and A. Govindjee, "Iterative repair planning for spacecraft operations in the ASPEN system," *ISAIRAS*, vol. 6, 1999.

[3] M. D. Rayman, P. Varghese, D. H. Lehman, and L. L. Livesay, "Results from the Deep Space 1 technology validation mission," *Acta Astronautica*, vol. 47, no. 2-9, pp. 475–487, 2000.

[4] R. Creasey, "Implementing spacecraft autonomy using discrete control theory," *46th International Astronautical Congress*, vol. 16, no. 2, pp. 109–116, 2013.

[5] G. Rabideau, S. Chien, R. Sherwood et al., "Mission operations with autonomy: a preliminary report for Earth Observing-1," in *International Workshop on Planning and Scheduling for Space (IWPSS)*, pp. 22–25, Darmstadt, Germany, 2004.

[6] D. Tran, S. Chien, G. Rabideau, and B. Cichy, "Flight software issues in onboard automated planning: lessons learned on EO-1," in *International Workshop on Planning and Scheduling for Space (IWPSS)*, pp. 1–7, Darmstadt, Germany, 2004.

[7] R. Sherwood, S. Chien, and D. Tran, "Autonomous science agents and sensor webs: EO-1 and beyond," in *IEEE Aerospace Conference (IAC)*, pp. 1–10, Big Sky, MT, USA, 2004.

[8] G. Rabideau, D. Tran, S. Chien et al., "Mission operations of Earth Observing-1 with onboard autonomy," in *IEEE International Conference on Space Mission Challenges for Information Technology*, pp. 1–7, Pasadena, CA, USA, 2006.

[9] G. Rabideau, R. Knight, S. Chien, A. Fukunaga, and A. Govindjee, "Iterative repair planning for spacecraft operations in the ASPEN system," in *International Symposium on Artificial Intelligence Robotics and Automation in Space (ISAIRAS)*, pp. 99–106, NOORDWIJK, NETHERLANDS, 1999.

[10] G. Rabideau, B. Engelhardt, and S. Chien, "Using generic preferences to incrementally improve plan quality," in *International Conference on Artificial Intelligence Planning Systems (AIPS)*, pp. 236–245, Breckenridge, Colorado, 1999.

[11] C. Wang, J. Li, N. Jing, J. Wang, and H. Chen, "A distributed cooperative dynamic task planning algorithm for multiple satellites based on multi-agent hybrid learning," *Chinese Journal of Aeronautics*, vol. 24, no. 4, pp. 493–505, 2011.

[12] W. Chong, J. Ning, L. Jun, W. Jun, and C. Hao, "Cooperative co-evolutionary algorithm in satellite imaging scheduling of cooperative multiple centers," in *IEEE Congress on Evolutionary Computation*, pp. 1–8, Barcelona, Spain, 2010.

[13] D. Morgan, S.-J. Chung, and F. Y. Hadaegh, "Model predictive control of swarms of spacecraft using sequential convex programming," *Journal of Guidance, Control, and Dynamics*, vol. 37, no. 6, pp. 1725–1740, 2014.

[14] B. Du and S. Li, "A new multi-satellite autonomous mission allocation and planning method," *ACTA Astronautica*, vol. 63, pp. 287–298, 2019.

[15] S. Cheng, J. Chen, and L. Shen, "A MAS-based negotiation model and its application to multiple observation collaborative satellite planning," in *International Conference on Computer and Automation Engineering*, pp. 205–208, Singapore, 2010.

[16] C. Iacopino, P. Palmer, A. Brewer, N. Policella, and A. Donati, "EO constellation MPS based on ant colony optimization algorithms," in *2013 6th International Conference on Recent Advances in Space Technologies (RAST)*, pp. 159–164, Istanbul, Turkey, 2013.

[17] X. Gallud and D. Selva, "Agent-based simulation framework and consensus algorithm for observing systems with adaptive modularity," *Systems Engineering*, vol. 21, no. 5, pp. 432–454, 2018.

[18] A. Globus, J. Crawford, J. D. Lohn, and A. Pryor, "A comparison of techniques for scheduling earth observing satellites," in *Conference on Nineteenth National Conference on Artificial Intelligence*, pp. 836–843, San Jose, CA, USA, 2004.

[19] M. Campbell and T. Schetter, "Comparison of multiple agent-based organizations for satellite constellations," *Journal of Spacecraft and Rockets*, vol. 39, no. 2, pp. 274–283, 2002.

[20] T. Schetter, M. Campbell, and D. Surka, "Multiple agent-based autonomy for satellite constellations," *Artificial Intelligence*, vol. 145, no. 1–2, pp. 147–180, 2003.

[21] X. L. Deng, Y. F. Dong, and S. C. Xie, "Multi-granularity mission negotiation for a decentralized remote sensing satellite cluster," *Remote Sensing*, vol. 20, 2020.

[22] D. Ongaro and J. Ousterhout, "In search of an understandable consensus algorithm," in *USENIX Annual Technical Conference*, pp. 305–319, Philadelphia, PA, US, 2014.

[23] M. Castro and B. Liskov, "Practical Byzantine fault tolerance," in *Appears in the Proceedings of the Third Symposium on Operating Systems Design and Implementation*, pp. 1–14, Cambridge, MA, USA, 1999.

[24] V. Dhillon, D. Metcalf, and M. Hooper, "Recent developments in blockchain," *Blockchain Enabled Applications*, vol. 11, pp. 151–181, 2017.

[25] Y. Yao, "Three-way decision: an interpretation of rules in rough set theory," in *Rough Sets and Knowledge Technology. RSKT 2009*, pp. 642–649, 2009.

[26] Y. Yao, "Three-way decisions with probabilistic rough sets," *Information Sciences*, vol. 180, no. 3, pp. 341–353, 2010.

[27] Y. Yao, "The superiority of three-way decisions in probabilistic rough set models," *Information Sciences*, vol. 181, no. 6, pp. 1080–1096, 2011.